Carbon 98 (2016) 484–490

Contents lists available at ScienceDirect

Carbon

journal homepage: www.elsevier.com/locate/carbon

THz TDS study of several sp^2 carbon materials: Graphite, needle coke and graphene oxides

Pedro Chamorro-Posada [a, *], José Vázquez-Cabo [b], Óscar Rubiños-López [b], Jesús Martín-Gil [c], Salvador Hernández-Navarro [c], Pablo Martín-Ramos [c], Francisco M. Sánchez-Arévalo [d], Albert V. Tamashausky [e], César Merino-Sánchez [f], Roberto C. Dante [g]

[a] Dept. de Teoría de la Señal y Comunicaciones e Ingeniería Telematica, Universidad de Valladolid, ETSI Telecomunicación, E-47011, Valladolid, Spain
[b] Dept. de Teoría de la Señal y Comunicaciones, Universidad de Vigo, EI Telecomunicación, Campus Universitario, E-36310, Vigo (Pontevedra), Spain
[c] Advanced Materials Laboratory, ETSIIAA, Universidad de Valladolid, Avda. de Madrid 44, 34004, Palencia, Spain
[d] Instituto de Investigaciones en Materiales, Universidad Nacional Autónoma de México, Circuito Exterior, Ciudad Universitaria, Coyoacán, 04510, D.F., Mexico
[e] Technical Services, Asbury Carbons Inc. 405 Old Main St, Asbury, NJ, 08802, USA
[f] Grupo Antolín Ingeniería S.A., Crta Madrid-Irún, km. 244.8, Burgos, Spain
[g] Nanomaterials and Simulation Lab, Facultad de Mécanica, Escuela Politecnica Nacional, Ladrón de Guevara E11 – 253, Quito, Ecuador

ARTICLE INFO

Article history:
Received 28 August 2015
Received in revised form
25 October 2015
Accepted 5 November 2015
Available online 17 November 2015

ABSTRACT

Terahertz time-domain spectroscopy has been used to probe the properties of four carbon allotropes with a sequenced *c*-axis stacking order: single-layer reduced graphene oxide, few-layer graphene oxide, disordered needle coke and highly organized graphite. The results obtained demonstrate a very high sensitivity to the structural characteristics of the tested samples. The multi-layer materials show the same type of spectral response with strong variations in the attenuation in the whole terahertz band depending on their constructural organization. The single-layer sample shows a distinct response where conductive effects dominate. The results obtained are consistent with theoretical investigations using semi-empirical quantum chemistry methods.

1. Introduction

Carbon-based materials play a key role in science and technology. Graphites find a vast range of industrial and research applications due to their mechanical, thermal, electrical and chemical properties [1]. Carbon nanostructures, such as fullerenes or carbon nanotubes, are at the focus of an intense research activity. Among them, the impact of graphene [2] in materials science seems to be ever-growing. Its outstanding electrical and optical properties [3] make it ideal for the development of new devices in optoelectronics and photonic applications ranging from the THz band [4] to microwave photonics [5], nonlinear optics [6] and magneto-optics [7]. The incorporation of graphene in metamaterial structures permits to develop tunable devices for the near infrared or the terahertz spectral regions [8,9]. High quality graphene can be produced by means of chemical vapor deposition on metal substrates [10,11] or by epitaxial growth on silicon carbide via silicon sublimation [12,13]. However, the cost-effective mass-production of graphene and graphene-like materials is typically based on the mechanical exfoliation of graphite or on the preparation of graphene oxides (GO) by chemical oxidation of graphite and subsequent exfoliation in water [14].

Besides X-ray diffraction and microscopic examination techniques, a broad range of spectroscopic methods are routinely used for the structural characterization of carbon materials [1]. These include surface analyses (X-ray photoelectron spectroscopy, Auger electron spectroscopy and angle-resolved photoemission spectroscopy) and vibrational characterization (Raman and infrared spectroscopy). Photoluminescence excitation spectroscopy is also very commonly used in the characterization of carbon nanotubes. Measurement techniques that permit to identify and characterize

* Corresponding author.
E-mail address: pedcha@tel.uva.es (P. Chamorro-Posada).

http://dx.doi.org/10.1016/j.carbon.2015.11.020
0008-6223/

the members of the carbon family in a fast and accurate manner are essential to carbon research and applications. Raman spectroscopy is particularly versatile in the determination of the morphological properties of carbon allotropes [15]. Not only it is amongst the most commonly used characterization tools in carbon research but it also has become nearly a standard in the case of graphene. Infrared spectroscopy has a complementary character in relation with Raman spectroscopy due to the mutually exclusive character of Raman and optically active resonances resulting from the electric dipole selection rules.

Terahertz time-domain spectroscopy (THz-TDS) [16] is an emerging characterization technique that provides very useful information on the structural organization of materials that is not available by other means. In this spectral region, optically active vibrational modes corresponding to long-range interactions can be detected in large molecular systems [17,18]. This information can be very useful, for instance, to determine the structural properties of polymers [19]. In a previous study [20], we showed that THz-TDS can be employed to analyse in a very effective manner the transition from a 2D to a 3D organization of a carbon nitride polymer. THz-TDS has also been used in the characterization of pristine epitaxially grown multilayer graphene [21], distinct from the type of materials addressed by us, by detecting the change in the conductivity with the number of graphene layers.

In this work, several carbon allotropes have been studied using THz-TDS. Naturally, this survey is not exhaustive due to the very large number of members in the family of carbon materials. Instead, we have chosen a few substances that range in their structural organization along the *c* axis from 2D framed reduced graphene oxide to highly ordered 3D graphite. Former studies on the optical properties of carbon-based materials in the THz spectral region have focused mostly on the shielding properties of carbon composites to electromagnetic radiation [22] or on the use of carbon nanomaterials for the development on new devices in the THz band [23]. Our aim is the evaluation of THz-TDS as a spectroscopic tool for the fast identification of materials and the characterization of their structural properties. The results show a clearly distinct type of spectra in the 2D reduced graphene oxide, dominated by conductive effects. The other tested materials, which show a varying degree of organization in their constitutive 3D piling of carbon layers, share the same type of spectral response. In this latter case, the THz attenuation varies strongly for the different tested materials and its intensity is consistently correlated with their stacking order. Given its high sensitivity for obtaining information on long-range structural characteristics, this spectral technique can be deemed as a promising tool for fast and inexpensive quality assessment in the lab- and mass-production of carbon-related materials and graphenes in particular. Finally, we also propose an interpretation of the results based on the analysis of the THz vibrational resonances of graphite and graphene obtained from quantum chemistry semi-empirical computations and we put forward a model for the spectral response of reduced graphene oxide dominated by conductive effects in finite size domains.

2. Materials, experimental and theoretical methods

2.1. Materials

Natural flake graphite (Asbury grade micro 850) and calcined petroleum needle coke (Asbury 4055) were supplied by Asbury Carbons Inc.

High quality graphene oxide (GO), produced from helical-ribbon carbon nanofibres by chemical methods, was supplied by Grupo Antolín Ingeniería (GRAnPH). The sample consists of few layer (up to five) graphene oxide nanoplatelets, highly crystalline and large cross section (above 10 square microns) [24].

Reduced graphene oxide (rGO), chemically reduced from graphene oxide (GO), was supplied by Graphenea. The sheet dimension is variable, the carbon content ranges from 77 to 87% and it features an electrical conductivity >600 S/m [25].

The materials under study were dispersed in polyethylene (PE) powder in a variable low concentration and the mixture was thoroughly milled in an agate mortar. Ultra-high molecular weight surface-modified, 53–75 μm particle size PE from Sigma–Aldrich was employed. The resulting samples were pressed, using a Graseby Specac press at CACTI (University of Vigo), to form pellets with a diameter of 13 mm.

Fig. 1 shows SEM images of the materials used in this work. Both natural flake graphite and calcined petroleum needle coke have a proper 3D organization resulting from the staking of a large number of sp^2 carbon layers. The powder X-ray patterns displayed in Fig. 2 illustrate the structural differences between an organized graphitic carbon and the amorphous needle coke. It is noteworthy to point out that needle coke can be considered a graphite precursor, since exhibits a certain degree of stacking along the *c* direction but a larger interplanar distance (lower interplanar interaction) as it can be inferred from the 002 reflection angle (25.8°), lower than that of graphite. However, the layered structure of needle coke can be appreciated in Fig. 1b. The broadness of the 002 peak of needle coke also indicates that the number of ordered stacked graphene sheets is much lower than for graphite. In a certain way, needle coke can be seen as an intermediate between a large series of stacked graphene sheets, such as graphite, and a material composed of few graphene sheets. TEM images of GO and rGO are compared side by side in Fig. 3 where the distinct single-layer character of rGO can be contrasted with the multilayer structure of the GO sample that displays a small varying number of layers.

2.2. THz time domain spectroscopy measurements

A Menlo Tera K15 Spectrometer was used for the THz-TDS analysis. The system is based on a 1560 nm fiber laser that generates 90 fs pulses at a repetition rate of 100 MHz. This provides a compact fiber-coupled setup. The system was operated in a nitrogen rich atmosphere in order to avoid the signature of water absorption in the recorded traces. Ten sample and ten reference measurements were performed in each case in order to reduce the noise in the measurements.

The material parameters in the spectral range of interest were calculated from the time domain photocurrent traces measured with the spectrometer. These time domain waveforms depend not only on the material but also on the width of the pellets, due to the contributions from multiple reflections at the pellet–air interfaces. Signal processing techniques similar to those described by Duvillaret et al. [26] were employed in order to obtain the THz spectra of the materials.

It is important to point out that pulsed signals used in THz-TDS impose an intrinsic reduction of the dynamic range as the frequency grows that, in the presence of very broad attenuation regions typical of disordered media, can artificially shape the measured spectrum creating the wrong impression of the presence of a resonant peak [27]. For all the measurements presented in our study, it has been checked that in the displayed spectral range the level of the signal received after propagation through the sample is above the noise floor. Even though we have used our own software for the estimation of the material parameters, this test has been confirmed using the commercial software Teralyzer (Menlo Systems).

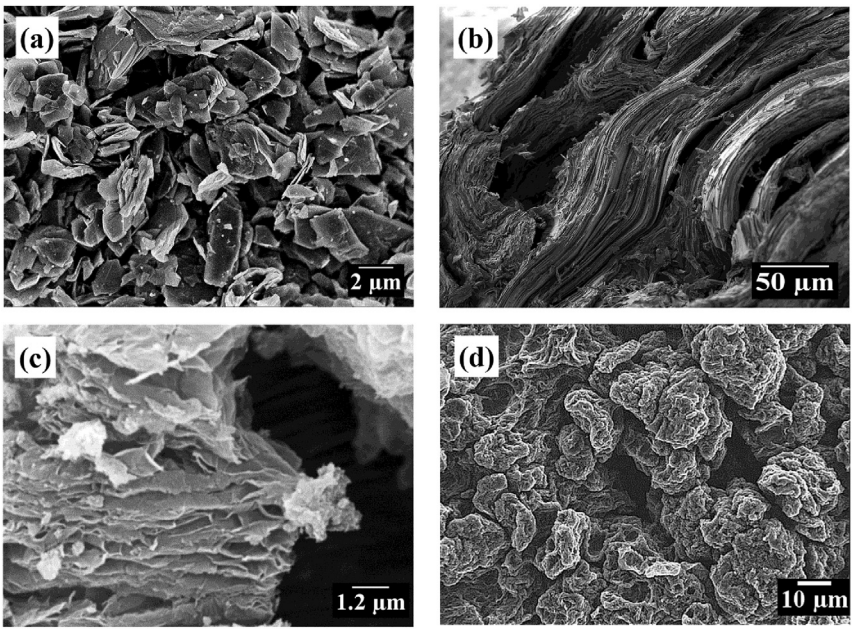

Fig. 1. SEM images of the materials used in this study: (*a*) Asbury natural flake graphite, (*b*) Asbury needle coke, (*c*) Antolin graphene oxide and (*d*) Graphenea reduced graphene oxide. The structural order displayed by the samples along the *c* axis ranges from the single-layer character of reduced graphene oxide (d) to the highly organized natural flake graphite (a). The few-layer Antolin graphene oxide (c) and needle coke (b), with a lower degree of structural organization than graphite, complete the sequence.

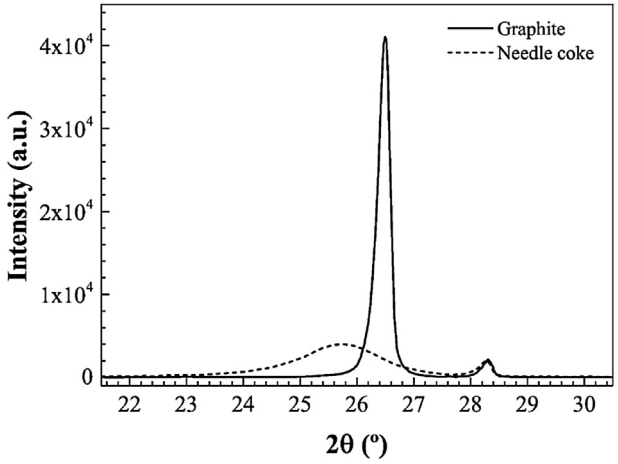

Fig. 2. X-ray powder diffraction scans of graphite and needle coke. The results show the structural differences between graphitic carbon and needle coke. The 002 reflection angle in needle coke is lower and less defined than in graphite, indicating a lower degree of the stacking order and a larger interplanar distance along the c axis in the needle coke.

2.3. Theoretical modeling of the THz response

According to Drude model [28], a conductive material is characterized by the existence of an independent electron gas in the presence of atomic scattering centers and displays a complex conductivity

$$\sigma(\omega) = \frac{\varepsilon_0 \omega_p^2 \tau}{1 + j\omega\tau} \tag{1}$$

where ε_0 is the dielectric permittivity of vacuum and ω_p is the plasma frequency. Electron scattering events depend on the distance between scattering centers and the velocity of electrons, but they are assumed to be described by a constant rate $1/\tau$. In the low frequency limit $\omega\tau \ll 1$, the conduction is of ohmic character, dominated by the scattering events, and the conductivity becomes approximately real and constant $\sigma(\omega) \simeq \sigma_0$. For very high frequencies, the oscillatory displacements of the electrons under the effect of an electric field is much smaller than the average distance between scattering centers and the electron gas behaves like a plasma with an imaginary conductivity of magnitude monotonically decreasing with frequency. In the THz band, Drude model has been shown to account for electronic transport properties in supported graphene [29] due to electron-impurity scattering.

In the absence of resonant polarization effects in the spectral region of interest, an effective relative permittivity $\varepsilon_r = \varepsilon / \varepsilon_0$ can be defined from Ampère-Maxwell law given by

$$\varepsilon_r(\omega) = \varepsilon_{r,\infty} - j\frac{\sigma(\omega)}{\omega\varepsilon_0}, \tag{2}$$

where $\varepsilon_{r,\infty}$ is a constant (real) background dielectric permittivity. For a good conductor $\sigma \simeq \sigma_0 \gg \omega\varepsilon_\infty$. Assuming a nonmagnetic medium, the complex propagation constant is $\gamma(\omega) = \alpha(\omega)/2 + jkn(\omega) = j\omega\sqrt{\mu_0\varepsilon(\omega)}$ and, upon substituting Eq (2), one obtains

$$\alpha(\omega)n(\omega) = \eta_0\sigma_R(\omega) \tag{3}$$

and

$$n(\omega)^2 - \left(\frac{\alpha(\omega)}{2k}\right)^2 = \varepsilon_{r,\infty} + \frac{\sigma_I(\omega)}{\omega\varepsilon_0} \tag{4}$$

where $\sigma = \sigma_R + j\sigma_I$, η_0 is the vacuum wave impedance and $k = \omega/c$ is the wavenumber. Equations (3) and (4) can be solved for n and α. For a good conductor, $\alpha(\omega) \simeq \sqrt{2\mu_0\sigma_0\omega}$ and $n(\omega) \simeq \sqrt{\sigma_0/(2\varepsilon_0\omega)}$.

A value of $1/\tau \simeq 40$ THz in the Drude model parameter has recently been reported for an rGO film [30] and, therefore, a real and constant value of the conductivity can be assumed for a spectral range up to a few THz. Our rGO samples, nevertheless, are

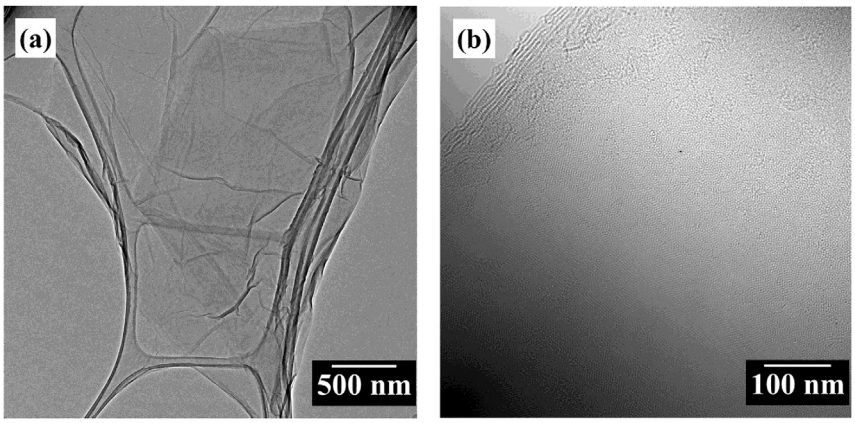

Fig. 3. TEM images of (a) Antolin graphene oxide and (b) Graphenea reduced graphene oxide. The few-layer composition of the material in (a) can be contrasted with the single-layer sheet of the sample displayed in (b).

shaped as small sheets of variable size and the impact of the sheet dimension on the conductivity has to be accounted for.

We consider rGO sheets with a real conductivity σ_0 and an average diameter d. For spectral components with a wavelength much shorter than d, electrons react as in a good conductor to the influence of an electric field, without any significant effect from the finite size of the sheets. If $\lambda \gg d$, on the other hand, the electrons behave essentially as bounded charges and we expect a polarization-like contribution from the complex conductivity in this regime. We put forward a phenomenological model for the conductivity contributed by rGO sheets of a given average diameter d, which is the simplest one that fulfills the requirements stated above:

$$\sigma(\omega) = \frac{j\omega\tau_d\sigma_0}{1 + j\omega\tau_d}. \tag{5}$$

As in the Drude model, we assume a constant average transit time τ_d for the electron motion within the boundaries of a rGO sheet that is related with the average sheet diameter and the electron velocity. Eq. (5) accounts for the finite-size effects at low frequencies. The model of Eq. (5) is intended to describe the material only in a limited frequency range and should be supplemented with other terms for a full description of the response. In particular, its impulse response corresponds to the differentiation of the Drude response, and is singular at $t = 0$. The introduction of additional terms in the spectral response should eliminate this singularity and guarantee the causality and the fulfillment of Kramers–Kronig relations of the overall transfer function.

Optically active vibration modes in the frequency band of interest produce resonant absorption contributions competing with conductive effects and give a total permittivity

$$\varepsilon_r(\omega) = \varepsilon_{r,p}(\omega) - j\frac{\sigma(\omega)}{\omega\varepsilon_0}. \tag{6}$$

In an amorphous material, short-range order can be largely responsible for the vibrational properties in the dielectric response, with a broadening of the associated spectral features [31]. The random fluctuations of the permittivity in disordered materials can introduce additional propagation loss through Rayleigh scattering, and the simultaneous presence of material disorder and vibration modes can result in resonance enhanced scattering. The behavior of disordered materials in the THz band is complex and its explanation still open to debate [32]. Disorder can shape terahertz absorption [33] in glassy materials producing universal broadband features. Numerical investigations have permitted to identify the interaction between resonant vibrational modes with the extended far-infrared phonons [34] as the underlying mechanism producing the broad THz attenuation spectra characteristic of disordered media. A similar role played by librational resonances in orientational glasses has been studied in Ref. [35].

Former studies on different types of graphitic and graphenic materials and their derivatives in the THz region [22,23] have focused mainly on their conductive properties. Here, we address the THz properties of materials with the emphasis placed on the broad attenuation bands with a polarization origin that is characteristic of disordered materials in this spectral region.

2.4. Quantum chemistry computations

The semiempirical quantum chemistry computations were performed with the PM7 method [36] using the parallel implementation for shared-memory CPUs [37] of the MOPAC2012 [38] software package. The numerical calculations were performed in a Debian Linux server with 128 GB of RAM and four AMD Opteron 6274 processors with a CPU clock of 2.2 GHz and 16 cores per processor.

PM7 belongs the family of neglect of diatomic differential overlap (NDDO) semi-empirical methods and corresponds to a recent parametrization improving the former PM6 scheme. These methods are based on the use of approximations to avoid computationally intensive steps and empirically determined parameters to obtain the best fit of predicted results to a training set of reference data. The result is a reduced computational load, when compared to *ab-initio* methods, and high predictive power for chemical systems adequately treated in the training set. These methods typically show good performance in the description of Organic Chemistry, where a few elements are used extensively, and, in particular, in Carbon Chemistry.

3. Results

3.1. Measurements

The measured THz spectra for the natural flake graphite, GO and the needle coke are shown in Fig. 4. As described in Section 2, the materials have been dispersed in a PE matrix due to their high absorption in the THz band. The same concentration of 2.5 wt% has been used in all cases. A reference measurement of the pure PE matrix is also shown in the figure. Even though PE has a resonance

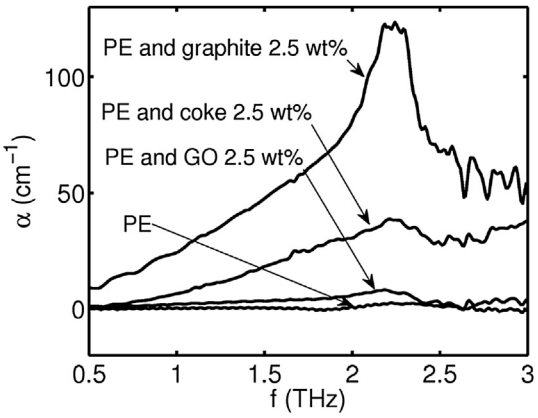

Fig. 4. Attenuation coefficient measured for the multi-layer materials under analysis: natural flake graphite and calcined petroleum needle coke in a PE matrix. The results show a direct correspondence between the attenuation in the THz band and the structural order of the samples.

in the same frequency band [19], its intensity is shown to be very small and it is not comparable with those of the materials under study. The measured spectra for rGO at 1.5 wt%, 2.5 wt% and 5 wt% in PE are depicted in Fig. 5.

The few-layer GO displays the same type of attenuation response that is found in natural flake graphite and in needle coke, but the intensity of the band is much lower. This absorption band is absent in single-layer reduced graphene oxide. The frequency dependence of both the refractive index and the attenuation for rGO resembles the characteristic response dominated by conductive effects (see Section 2.3) with $\alpha(f) \propto \sqrt{f}$ and $n(f) \propto 1/\sqrt{f}$. The assumption of a constant real conductivity and a constant background permittivity, nonetheless, provides a poor fit with the measurements. A good correspondence is obtained using the model of Eq. (5) that includes the effect of the finite size of the rGO sheets. The results of the least squares fit of the measured attenuation up to 1.7 THz using Eq. (3) are displayed in Fig. 5(a) with dashed lines. The measured real refractive index in this range has also been used to calculate the estimate of the attenuation. The obtained parameters show the expected increase of the conductivity with the rGO concentration: $\sigma_0 = 2.15$ S/m for 1.5 wt%, $\sigma_0 = 6.26$ S/m for 2.5 wt%, and $\sigma_0 = 10.60$ S/m for 5 wt% and little variation in τ_d with values of 2.94×10^{-13} s 3.66×10^{-13} s and 4.03×10^{-13} s for 1.5 wt%, 2.5 wt% and 5 wt%, respectively. The fit with the proposed model is excellent for frequencies between 0.5 THz and 2 THz. At 2.2 THz there is an attenuation peak that could be due to the interaction with the PE matrix or the presence of impurities in the sample. At higher frequencies, there is a monotonic increase of the attenuation with frequency that could be explained by the effect of Rayleigh scattering in the material or which may be the result of the higher frequency resonance found in our numerical calculations. An approximately constant refractive index up to 2 THz has been measured for the multilayer materials for which the attenuation coefficient is shown in Fig. 4. We stress that the shape of the spectra permits to clearly identify without ambiguity each of the tested materials using only the THz measurements.

3.2. Semi-empirical quantum chemistry computations

Both the graphite and graphene geometries were optimized using the semi-empirical PM7 method implemented in MOPAC assuming periodic boundary conditions. One period of the computational domain included 4×4 unit cells for graphene and $4 \times 4 \times 2$ unit cells for graphite, which corresponds to four layers. The geometry optimization was calculated to a high precision within the PM7 method by requiring the gradient norm to drop below 0.1 kcal/mol/Å as the terminating condition. The lattice data of the calculated geometry of graphite are $a = 2.458$ Å, $b = 2.458$ Å, $c = 7.074$ Å, $\alpha = 89.72°$, $\beta = 89.62°$ and $\gamma = 60.00°$, where a, b and c are the lengths of the crystal unit cell edges and α, β and γ the angles between them. The theoretically obtained lattice parameters are in good agreement with their actual values [39].

The vibrational spectra associated with the optimised geometries for graphene and graphite were also studied using MOPAC with the PM7 Hamiltonian. This analysis confirms that the calculated geometries correspond to true ground states. Fig. 6(a) shows the computed vibrational frequencies and their intensities for graphite in the band between 1 THz and 2.2 THz. The vibration modes are identified with the nR symmetry labels assigned by MOPAC, where R is the irreducible representation and n is the nth occurrence of that representation. An estimate for the THz absorption curve assuming a Lorentzian lineshape, obtained using Gabedit [40], has also been plotted with a solid line. This representation is just intended to guide the eye when reading the figure. The vibration modes, with a dominant contribution in the region between 2 and 2.2 THz, are depicted in Fig. 6(b–d), where the

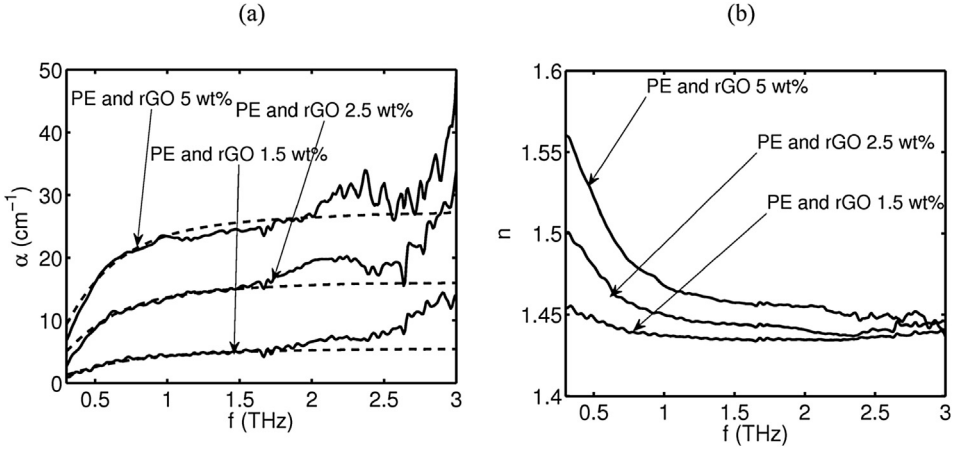

Fig. 5. Attenuation coefficient (a) and refractive index (b) measured for rGO at different concentration values in a PE matrix. Dashed lines correspond to the fits with the conductivity model of Eq. (5).

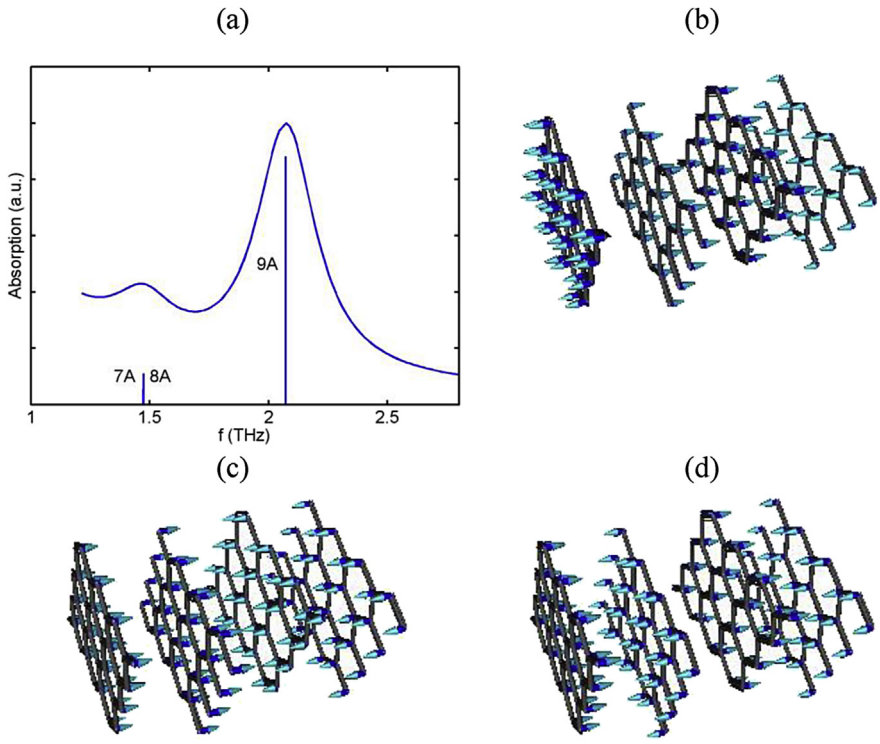

Fig. 6. (a) Frequencies and intensities of the vibrational modes in the band analysed using semi-empirical quantum chemistry calculations. (b) to (d) Displacements corresponding to the vibrational modes contributing to the absorption in the THz band shown in (a). (b) is mode 7A, (c) is 8A and (d) 9A. The arrows describing the displacements corresponding to the vibration modes have been magnified. (A color version of this figure can be viewed online.)

representations have also been made using Gabedit. The arrows describing the atomic displacements have been magnified in relation with the actual values. Calculations for graphene using the PM7 method do not show any vibrational resonance in this THz band. Starting from DC, the first vibrational mode is predicted at 5.07 THz, very far from the graphite resonances.

The THz vibrations of graphite calculated for this band correspond to the oscillation of the graphene layers, with all the atoms in the layer plane moving together. Vibrations shown in Fig. 6(b) and (d) are very similar and differ only in the relative phases of the movements of pairs of adjacent planes. Whereas in (d) the two pairs approach and separate simultaneously, in (b) one pair increases its separation while in the adjacent pair the separation between planes diminishes. Only the dominant vibration in Fig. 6(a) corresponds to a fundamental $k = 0$ vibration mode, whereas the other two modes appear due to the extension of the computational domain over 2 unit cells in the c direction. The consideration of a larger computational domain could introduce more complex interplanar vibrations, presumably in the same frequency band. Nevertheless, we stress that the dominant mode in these calculations corresponds to the most basic oscillation, where pairs of adjacent planes approach or separate simultaneously. These resonances are obviously absent in the calculations performed for single-layer graphene.

4. Discussion

The measured THz spectra could be the result of the presumable existence of the type of inter-planar vibrations predicted by the semi-empirical calculations for graphite in this band, since a greater degree of stacking order is expected to enhance the contribution from these modes. This would explain the qualitative differences between the spectrum of single-layer sheets of rGO and the rest of materials that share a multi-layer structure. Possible mechanisms for producing the broad attenuation spectra shown in Fig. 4 include the interaction of the vibrations with the extended phonons and resonance enhanced Rayleigh scattering, as discussed in Section 2.3.

The measured spectra also display a very large variation of the intensity of the attenuation between the natural flake graphite and the needle coke. This is can be attributed to the differences in the stacking order along the c direction between the two materials, where a more regular organization can be found for the natural flake graphite. Needle coke shows an interesting characteristic intensity absorption intermediate between graphite and multi graphene layered materials (GO), in good agreement with its intermediate order in the c direction.

There exists an appealing correspondence between the experimental spectra of Fig. 2 and the theoretical predictions, with a strong dominance from a probable vibration mode between 2 and 2.5 THz that reinforces our interpretation of the results. Even though we have thoroughly checked validity of the measurements presented in this study, this type of features must be treated with extreme care, as discussed in Section 2.2, since the characterization method has an intrinsic reduction in the dynamic range as the frequency grows that can produce an artifact with the shape of a broad peak in the presence of an extensive attenuation region at the upper end of the frequency range of the spectrometer. In any case, the vibrations described could produce extremely broadened features due to material disorder and the measurement of a well-defined peak is not a requirement to confirm their impact on the attenuation response.

Alternative physical phenomena could explain the measurements. For instance, Rayleigh scattering due to the fluctuations in the material properties could also produce the observed spectra. However, the size of the optical wavelength $\lambda \sim 150$ μm and that of

the PE particles suggest that the scale of the variation of the properties of the host matrix determined by the particle size should dominate the Rayleigh scattering in this band over those of the test carbon materials. Nonetheless, no such scattering has been observed in the reference measurements of PE. In addition, an explanation for the broad attenuation bands based on disorder of the sample material alone is inconsistent with the lower attenuation intensity of coke relative to that of graphene and the higher disorder of the former evidenced by XRD measurements.

5. Conclusion

A study of the far infrared spectra of four sp^2 carbon materials with a varying stacking order has been conducted using THz-TDS. GO displays the same type of attenuation, at a smaller intensity, exhibited by natural flake graphite and needle coke. Needle coke shows an intermediate behavior between those of graphite and GO whereas the spectral response of the essentially 2D rGO is clearly distinct and dominated by conductive effects. At the light of the measurements shown in Figs. 4 and 5 alone, it can be concluded that THz-TDS features a high sensitivity to the structural ordering of carbon allotropes, which qualifies it as a very efficient, fast and reliable characterization technique for assessing their production. We have also proposed a possible explanation of the observed results based on the theoretical predictions of the vibrational spectra in this band obtained with semi-empirical calculations (PM7 Hamiltonian).

Acknowledgments

This work has been supported by the Spanish National Research and Development Program and European Regional Development Fund (ERDF) under project Terasense grant number CSD2008-00068 (Consolider-Ingenio 2010), by the Spanish Government under project TACTICA and by ERDF and the Galician Regional Government under agreement for funding the Atlantic Research Center for Information and Communication Technologies (AtlantTIC). Grupo Antolin participates in the Graphene Flagship European initiative. The UVa group acknowledges support from Junta de Castilla y León grant numbers VA300A12-1 and VA036A12-2.

References

[1] P. Mukhopldhyay, R.K. Gupta, Graphite, Graphene and their Polymer Nanocomposites, CRC Press, Boca Raton, 2013.
[2] A.K. Geim, K.S. Novoselov, The rise of graphene, Nat. Mater. 6 (2007) 183–191.
[3] F. Bonaccorson, Z. Sun, T. Hasan, A.C. Ferrari, Graphene photonics and optoelectronics, Nat. Phot. 4 (2010) 611–622.
[4] B. Sensale-Rodríguez, R. Yan, L. Liu, D. Jena, H.G. Xing, Graphene for reconfigurable terahertz optoelectronics, Proc. IEEE 107 (7) (2013) 1705–1716.
[5] J. Capmany, D. Domenech, P. Muñoz, Graphene integrated microwave photonics, J. Light. Technol. 32 (20) (2014) 3785–3796.
[6] K. Kim, S.-H. Cho, C.-W. Lee, Nonlinear optics: graphene-silicon fusion, Nat. Phot. 6 (2012) 502–503.
[7] I. Crassee, J. Levallois, A.L. Walter, M. Ostler, A. Bostwick, E. Rotenberg, et al., Giant Faraday rotation in single- and multilayer graphene, Nat. Phys. 7 (2011) 48–51.
[8] X. He, Z.-Y. Zhao, W. Shi, Graphene-supported tunable near-IR metamaterials, Opt. Lett. 40 (2) (2015) 178–181.
[9] X. He, Tunable terahertz graphene metamaterials, Carbon 82 (2015) 229–237.
[10] L.G. De Arco, Y. Zhang, C.W. Schlenker, K. Ryu, M.E. Thompson, C.W. Zhou, Continuous, highly flexible, and transparent graphene films by chemical vapor deposition for organic photovoltaics, ACS Nano 5 (2010) 2865–2873.
[11] Z. Chen, W. Ren, L. Gao, B. Liu, S. Pei, H.-M. Cheg, Three-dimensional flexible and conductive interconnected graphene networks grown by chemical vapour deposition, Nat. Mater. 10 (2011) 424–428.
[12] Z.H. Ni, W. Chen, X.F. Fan, J.L. Kuo, T. Yu, A.T.S. Wee, Z.X. Shen, Raman spectroscopy of epitaxial graphene on a SiC substrate, Phys. Rev. B 77 (2008) 115416.
[13] T. Ohta, F. El Gabaly, A. Bostwick, J.L. McChesney, K.V. Emtsev, A.K. Schmid, T. Seyller, et al., Morphology of graphene thin film growth on SiC(0001), New J. Phys. 10 (2008) 023034.
[14] Y.-L. Zhang, L. Guo, H. Xia, Q.-D. Chen, J. Feng, H.-B. Sun, Photoreduction of graphene oxides: methods, properties and applications, Adv. Opt. Mater. 2 (1) (2014) 10–28.
[15] A.C. Ferrari, Raman spectroscopy of graphene and graphite: disorder, electron-phonon coupling, doping and nonadiabatic effects, Solid State Commun. 143 (2007) 47–57.
[16] S.L. Dexheimer, Terahertz Spectroscopy: Principles and Applications, CRC Press, Boca Raton, 2008.
[17] T.R. Globus, D.L. Woolard, T. Khromova, T.W. Crowe, M. Bykhovskaia, B.L. Gelmont, et al., THz-spectroscopy of biological molecules, J. Biol. Phys. 29 (2003) 89–100.
[18] D.L. Woolard, T.R. Globus, B.L. Gelmont, M. Bykhovskaia, A.C. Samuels, D. Cookmeyer, et al., Submillimiter-wave phonon modes in DNA macromolecules, Phys. Rev. E 65 (2003) 651903.
[19] S. Wietzke, C. Jansen, M. Reuter, T. Jung, D. Kraft, S. Chatterjee, et al., Terahertz spectroscopy on polymers: a review of morphological studies, J. Mol. Struct. 1006 (1–3) (2011) 41–51.
[20] P. Chamorro-Posada, J. Vázquez-Cabo, F.M. Sánchez-Arévalo, P. Martín-Ramos, J. Martín-Gil, L.M. Navas-Gracia, R.C. Dante, 2D and to3D transition of polymeric carbon nitride nanosheets, J. Solid State Chem. 219 (2014) 232–241.
[21] I.-T. Lin, J.-M. Liu, K.-Y. Shi, P.-S. Tseng, K.-H. Wu, C.-W. Luo, L.-J. Li, Terahertz optical properties of multilayer graphene: experimental observation of strong dependence on stacking arrangements and misorientation angles, Phys. Rev. B 86 (2012) 235446.
[22] L. Liu, A. Das, C.M. Megaridis, Terahertz shielding of carbon nanomaterials and their composites – a review and applications, Carbon 69 (2014) 1–16.
[23] R.R. Hartmann, J. Kono, M.E. Portnoi, Terahertz science and technology of carbon nanomaterials, Nanotechnology 25 (2014) 322001.
[24] J. Vera-Agullo, H. Varela-Rizo, J.A. Conesa, C. Almansa, C. Merino, I. Martin-Gullon, Evidence for growth mechanism and helix-spiral cone structure of stacked-cup carbon nanofibers, Carbon 45 (2007) 2751–2758.
[25] Graphenea Reduced Graphene Oxide Product Datasheet. Available: http://cdn.shopify.com/s/files/1/0191/2296/files/Graphenea_rGO_Datasheet_2014-03-25.pdf?2923.
[26] L. Duvillaret, F. Garet, J.L. Coutaz, A reliable method for extraction of material parameters in terahertz time-domain spectroscopy, IEEE J. Sel. Top. Quantum Electron 2 (3) (1996) 739–746.
[27] P.U. Jepsen, B.M. Fisher, Dynamic range in terahertz time-domain transmission and reflection spectroscopy, Opt. Lett. 30 (2005) 29–31.
[28] N.W. Ashcroft, N.D. Mermim, Solid State Physics, Harcourt, Orlando, 1974.
[29] N. Sule, K.J. Willis, S.C. Hagness, I. Knezevic, Terahertz-frequency electronic transport in graphene, Phys. Rev. B 90 (2014) 045431.
[30] J.T. Hong, K.M. Lee, B.H. Son, S.J. Park, D.J. Park, et al., Terahertz conductivity of reduced graphene oxide films, Opt. Express 21 (2013), 7663–7640.
[31] S.R. Elliot, Physics of Amorphous Materials, Longman, New York, 1983.
[32] W. Kob, D. Binder, Glassy Materials and Disordered Solids: an Introduction, World Scientific, London, 2011.
[33] S.N. Taraskin, S.I. Simdyankin, S.R. Elliot, J.R. Neilson, T. Lo, Universal features of terahertz absorption in disordered materials, Phys. Rev. Lett. 97 (2006) 055504.
[34] H.R. Schober, C. Oligscleger, Low-frequency vibrations in a model glass, Phys. Rev. B 53 (17) (1996) 11469–11480.
[35] M. Randeria, J.P. Sethna, Resonant scattering and thermal transport in orientational glasses, Phys. Rev. B 38 (17) (1988) 12607–12614.
[36] J.P.P. Stewart, Optimization of parameters for semiempirical methods VI: more modifications to the NDDO approximations and re-optimization of parameters, J. Mol. Mod. 19 (2013) 1–32.
[37] J.D.C. Maia, G.A.U. Carvalho, C.P. Mangueira, S.R. Santana, L.A.F. Cabral, G.B. Rocha, GPU linear algebra libraries and gpgpu programming for accelerating mopac semiempirical quantum chemistry calculations, J. Chem. Theory Comput. 8 (2012) 3072–3081.
[38] J.P.P. Stewart, Stewart Computational Chemistry, 2012. Colorado Springs, CO: USA, http://openmopac.net.
[39] O. Hassel, Ueber die Kristallstruktur des Graphits, Z. fuer Phys. 25 (1924) 317–337.
[40] A.R. Allouche, Gabedit-a graphical user interface for computational chemistry softwares, J. Comput. Chem. 32 (2010) 174–182.